# Anisotropy measurements in a multi-faced core sample by using pulse transmission method

Jaime Meléndez Martínez, Douglas R. Schmitt, and Randolph Kofman
Institute for Geophysical Research
Dept. of Physics, University of Alberta
Edmonton, Alberta, T6G 2E1
melendez@ualberta.ca

GeoConvention 2012:Vision

## Summary

Recent interest in unconventional reservoirs motivates our work in laboratory measurements of seismic anisotropy. Seismic anisotropy is the variation in speed of a wave as a function of its direction of propagation. Analyzing anisotropy in unconventional reservoirs is important since anisotropy leads, for example, to differential stresses upon loading and could affect hydraulic stimulation (Reinicke et al., 2010, Zimmermann and Reinicke, 2009); in this sense, laboratory measurements are an important tool to study seismic anisotropy at small scales which can aid in the characterization of larger formations.
The purpose of this work is to describe the laboratory methodology used to simultaneously measure ultrasonic P and S-waves in three different directions from a single core sample. Elastic anisotropy of a Proterozoic sedimentary rock from south-west Alberta is investigated. In metamorphic rocks seismic anisotropy is caused by preferred mineralogical alignment or foliation.

Assuming a transversally isotropic medium (VTI), arrays of compressional and shear piezoelectric ceramic transducers were mounted on a sample trimmed from a core to measure travel times of ultrasonic *P*-waves and *S*-waves as a function of confining pressure at directions perpendicular, parallel, and oblique to the plane of foliation (bedding). Results show that the sample is anisotropic and that microcracks play a minor role as a source of anisotropy which is mainly due to layering. Dependence of travel times and hysteresis effects can also be observed when pressurizing and depressurizing.

## Introduction

In this work, seismic anisotropy and its dependence on confining pressure are studied ultrasonically by using the pulse transmission method. The pulse transmission method is the most common method of ultrasonic measurements used to estimate velocities in geologic materials (Vernik and Liu, 1997; Dey-Barsukov et al., 2000; Mah and Schmitt, (2001a, 2001b); Wang, 2002b; Meléndez and Schmitt, 2011). This method involves generating and recording P and S ultrasonic waves traveling through a sample. Piezoelectric ceramic transducers with properly aligned polarizations are placed on each side of the sample so one of them plays the role of transmitter and the other one is the receiver. A fast-rise voltage is applied to the transmitter that sends a broad-band pulse (usually centered near 1 MHz) that propagates through the sample. When this pulse arrives to the receiver, a voltage is generated as a response to the pulse. The transit time through a sample is then picked from the recorded waveform. Knowing the length of the sample, the velocity of the wave can be easily calculated.

A method to measure anisotropy in a core sample that involves the pulse transmission method is the multi-core method (Meléndez and Schmitt, 2011) in which three plugs are cut, assuming a transversally isotropic medium, at the above mentioned directions and the travel times of the waveforms are measured independently in each of those directions. However, this method has the drawback that there is a possibility that the coring samples dissimilar heterogeneities of the main material and leads to incorrect results. To overcome this disadvantage a multi-faced cube method can be used, which has the advantage that possible heterogeneity problems are avoided since all of the waves propagate through the same sample. This method has been used by Kebaili and Schmitt (1997) and Mah and Schmitt (2001a, 2001b) to develop experimental methods to simulate walk-away VSP form blocks of acrylic and phenolic. In this work we propose to use it to simultaneously measure P and S velocities along the horizontal ($P_{90^o}$ and $SH_{90^o}$), vertical ($P_{0^o}$ and $S_{0^o}$) and 60° ($P_{60^o}$ and q-$SH_{60^o}$) with respect to the sample´s axis of symmetry, In order to recreate *in situ* pressure conditions similar to those in the Earth´s interior, the P-wave and the S-wave velocities are measured as a function of confining pressure by using a pressure vessel in two different cycles: compressing (Up Cycle) and decompressing (Down Cycle).

## Theoretical background

Phase velocities in a medium with vertical transverse isotropic symmetry (VTI) are given by (Thompsen, 1986):

$$V_P(\theta) = \left\{\frac{C_{11}sin^2(\theta) + C_{33}cos^2(\theta) + C_{44} + \sqrt{M}}{2\rho}\right\}^{\frac{1}{2}} \quad (1)$$

$$V_{SV}(\theta) = \left\{\frac{C_{11}sin^2(\theta) + C_{33}cos^2(\theta) + C_{44} - \sqrt{M}}{2\rho}\right\}^{\frac{1}{2}} \quad (2)$$

$$V_{SH}(\theta) = \left\{\frac{C_{66}sin^2(\theta) + C_{44}cos^2(\theta)}{\rho}\right\}^{\frac{1}{2}} \quad (3)$$

where $M = \{(C_{11} - C_{44})sin^2(\theta) - (C_{33} - C_{44})cos^2(\theta)\}^2 + (C_{13} + C_{44})^2 sin^2(2\theta)$, $\theta$ is the angle between the direction of propagation and the axis of symmetry, ρ is the bulk density of the sample, P is a compresional wave, SV and SH are polarized shear waves. $C_{11}, C_{33}, C_{44}, C_{66}$, and $C_{13}$ are the five elastic stiffnesses needed to describe a VTI medium.

Then from equations (1), (2) and (3) we have that:

$$C_{11} = \rho V^2_{P_{90^o}} \quad (4)$$

$$C_{33} = \rho V^2_{P_{0^o}} \quad (5)$$

$$C_{44} = \rho V^2_{S_{0^o}} \quad (6)$$

$$C_{66} = \rho V^2_{SH_{90^o}} \quad (7)$$

$$C_{13} = \left[\left\{\left(2\rho V_{P_{60^o}}^2 - \frac{3}{4}C_{11} - \frac{1}{4}C_{33} - C_{44}\right)^2 - \left(\frac{3}{4}C_{11} - \frac{1}{2}C_{44} - \frac{1}{4}C_{33}\right)^2\right\}\frac{4}{3}\right]^{\frac{1}{2}} - C_{44} \quad (8)$$

Equations (4) through (8) allow estimating elastic constants from recorded waveforms via the wave speeds so determined.

Using elastic constants Thomsen (1986) developed the so-called “Thomsen parameters” to quantified anisotropy in a VTI medium:

$$\varepsilon = \frac{C_{11} - C_{33}}{2C_{33}} \quad (9)$$

$$\gamma = \frac{C_{66} - C_{44}}{2C_{44}} \quad (10)$$

$$\delta = \frac{(C_{13} + C_{44})^2 - (C_{33} - C_{44})^2}{2C_{33}(C_{33} - C_{44})} \quad (11)$$

where $\varepsilon$ measures P-wave anisotropy, $\gamma$ measures SH-wave anisotropy. $\delta$ can be viewed as a measure of the anellipticity of the P wave curve (Cholach and Schmitt, 2006).

## Method

A sample was trimmed from a main core by using a rotating saw to obtain the three different orientations. Flat surfaces are needed to mount the piezoelectric transducers. In order to improve coupling between transducers and the sample and reduce noise, the trimmed surfaces were smoothed with both a spinning polisher and a fine grain sand paper.

1 MHz primary mode resonance P-wave and S-wave piezoelectric ceramic transducers were mounted on the previously smoothed surfaces. Since the polarization of the S-wave transducers is controlled by their orientation, a horizontally polarized shear wave $SH_{90^o}$ is obtained when the direction of particle motion is parallel to plane of foliation. A quasi horizontally polarized shear wave q-$SH_{60^o}$ is obtained when the direction of particle motion is $60^o$ with respect to layering. Polarization in the vertical direction ($S_{0^o}$) is irrelevant as long as the material is truly transversely isotropic. In this step proper alignment between S-wave transmitter and receiver transducers must be done. Figure 1 portrays the geometry of the P-wave and S-wave transducers mounted on the sample.

A thin strip of cooper acting as a ground (negative pole) is attached to the sample using quick epoxy. Once the quick epoxy is solidified the transducer is bonded to the strip cooper with a layer of conductive silver epoxy and on top on the transducer another strip of cooper (positive pole) is attached to the transducer with conductive silver epoxy. After conductive epoxy is solidified two wires are soldered on each piece of copper. Figure 2(a) shows a picture of the transducer´s set up. The sample is then sealed with urethane putty to avoid leakage of the confining pressure fluid into the sample as shown in Figure 2(b).

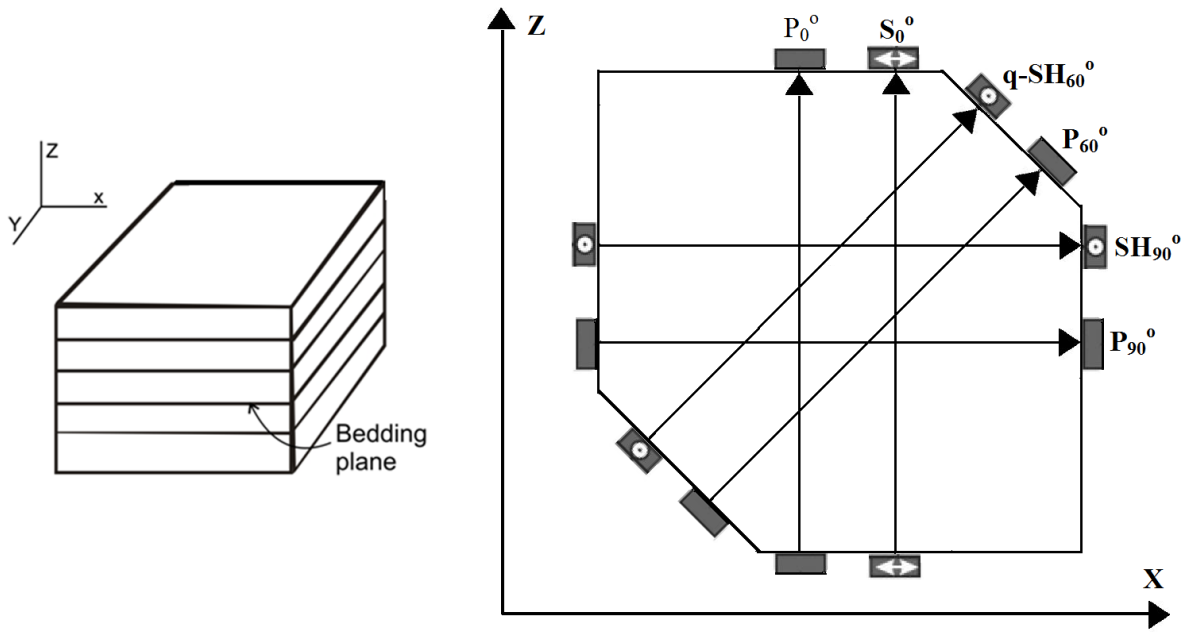


Figure 1. Schematic of the distribution of the piezoelectric transducers in the multi-faced method assuming a transversally isotropic medium. A S-wave is obtained in the vertical direction (perpendicular to bedding, 0 degrees), SH wave is obtained in the horizontal direction (parallel to bedding, 90 degrees) and quasi SH wave is obtained at an angle of 60 degrees with respect to bedding. P waves are obtained in all directions.

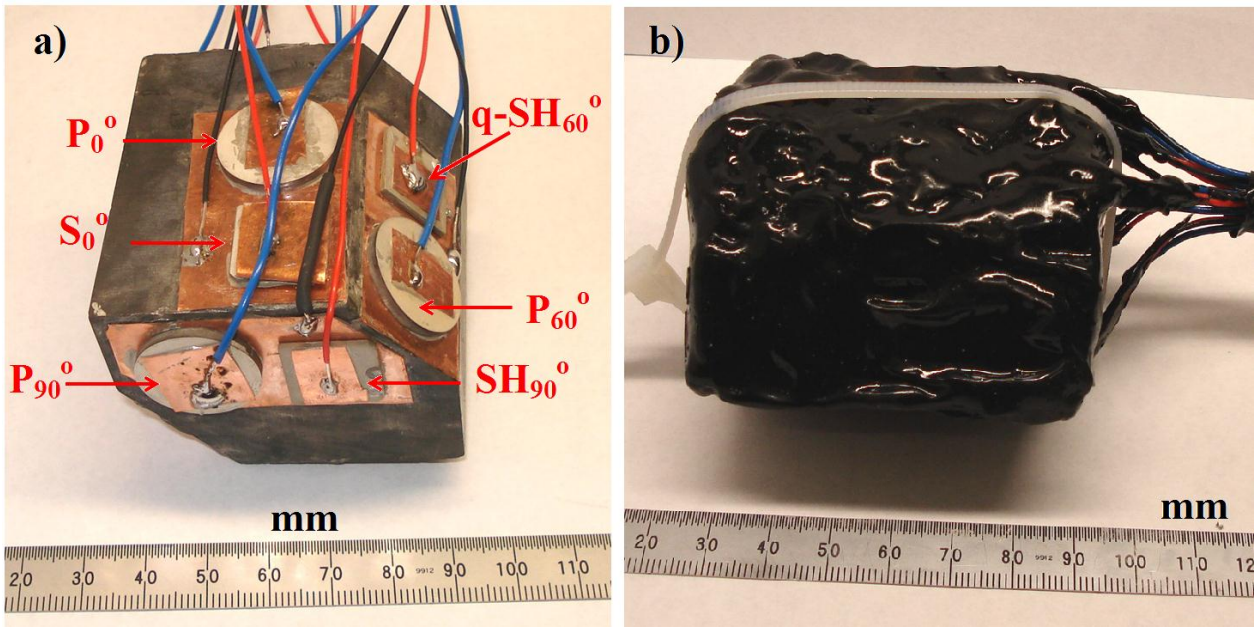


Figure 2. Photographs showing the piezoelectric transducers mounted on the sample (a) and sample sealed with urethane putty.

## *Experimental setup*

The experimental setup consists basically of a pulser generator/receiver system, a digital oscilloscope and a pressure vessel that can apply a confining pressure of up to 60 MPa (Figure 3). The transmitter is activated by applying a fast rising (5 ns) 200 V square wave to the piezoelectric ceramic which

produces a mechanical disturbance. The generated elastic wave is then recorded by the digital oscilloscope after travelling through the sample. Pressure was increased from 0 to 50 MPa in the compressing cycle and from 50 to 0 MPa in the decompressing cycle. The waveforms were recorded at approximately every 3 MPa increment.

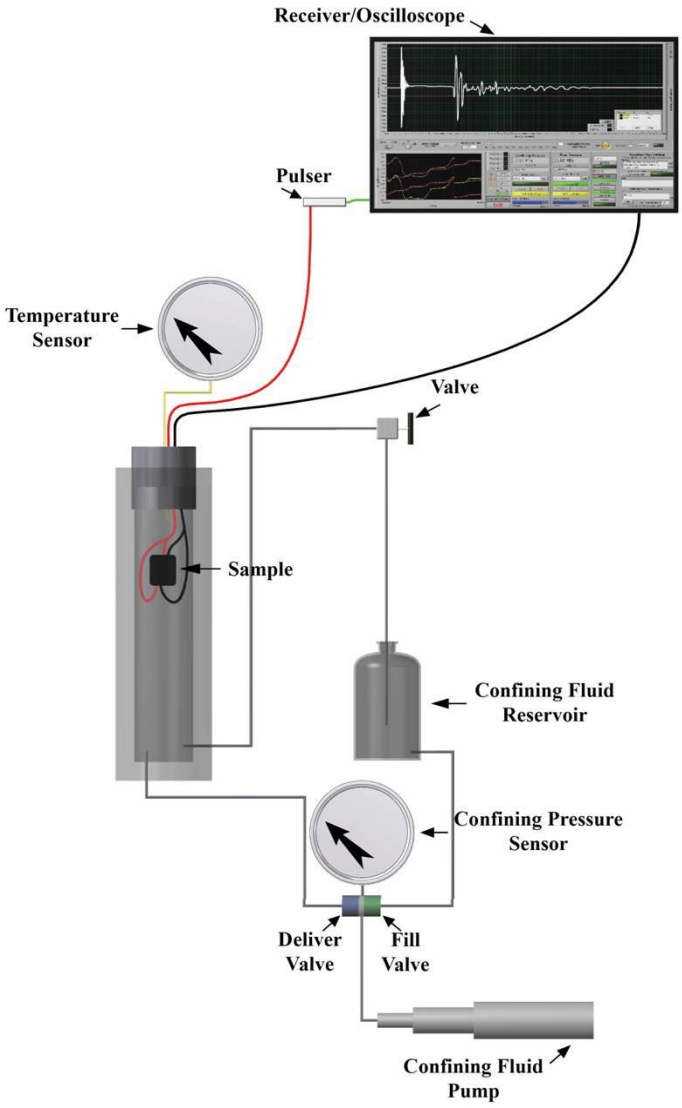


Figure 3. Experimental setup.

## Examples

Ultrasonic measurements were carried out on a meta-sedimentary rock sample. Some example *P*- and *S*-waveforms obtained in the test are shown in figure 4. Velocities obtained from waveforms in the three different directions versus confining pressure show VTI anisotropy (Figure 5). Travel times were measured both during pressurization and depressurization. An incremental change in velocity can be observed as pressure increased. In general, increase of velocities can be explained by closing microcracks and pores. Pressurization velocities are slower than depressurization velocities; this effect is called hysteresis (Gardner et al., 1965). When a sample is pressurized, microcracks and pores begin

closing at a certain rate; however, when depressurizing, due frictional forces, the opening rate of microcracks and pores is lower than the closing rate for a given pressure.

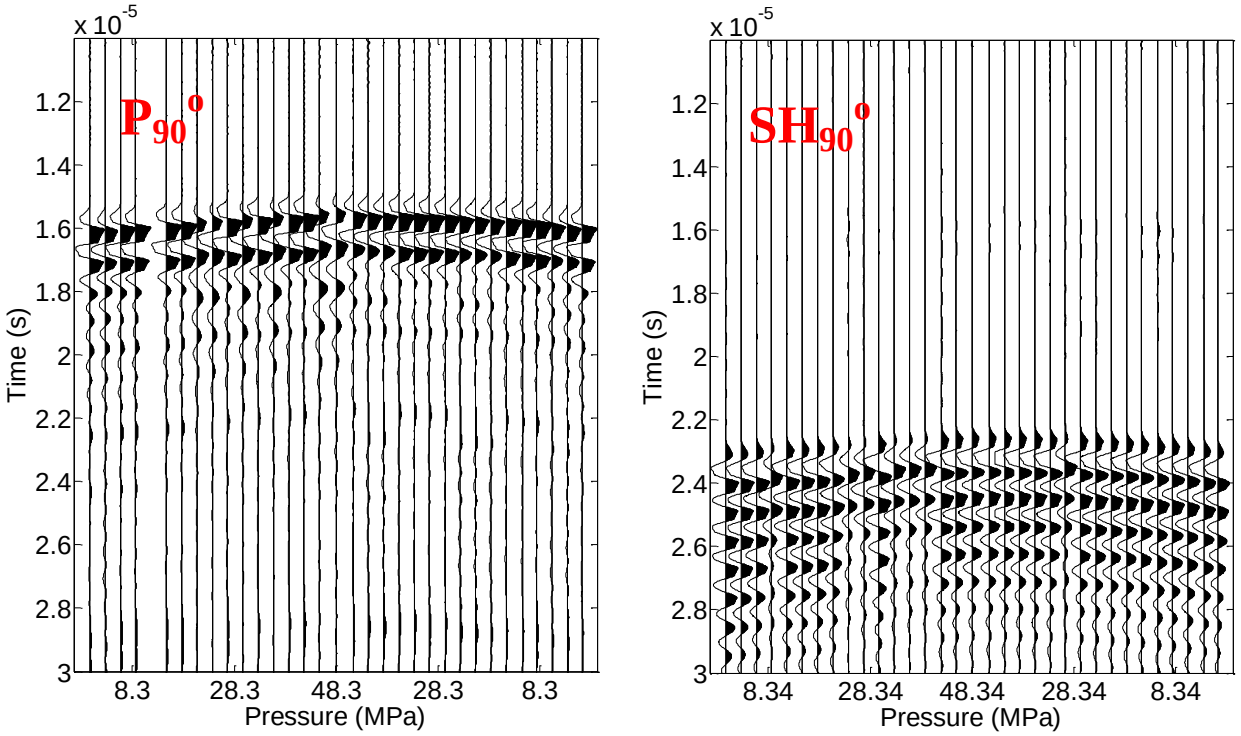


Figure 4. Suite of $P_{90}{}^{o}$ and $SH_{90}{}^{o}$ waveforms versus confining pressure.

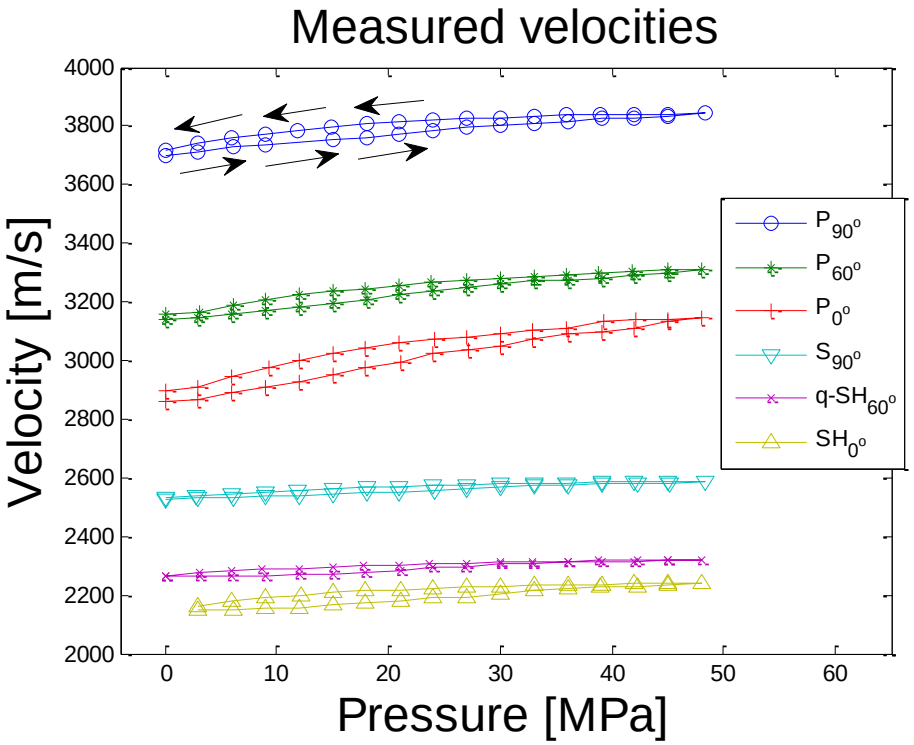


Figure 5. P- and S-wave velocities show VTI anisotropy. Arrows represent the evolution of measurements. Effect of hysteresis can be observed in the pressurization (up) and depressurization (down) cycles. Velocities increase as pressure increases.

Since microcracks have higher compliance than pores, microcracks close at relatively low pressures and affect velocities more than rounded pores (Kuster & Toksöz, 1974). In particular, a high gradient velocity increase at low pressures followed by a slow velocity increase at higher pressures characterizes a velocity increase due to microcracks (He, 2006). However; figure 5 shows that microcracks have a minor effect in the velocities since they appear to be stable (quasi lineal behavior) over the pressure range. The velocity gradient for the $SH_{90}^{o}$ -wave is only 59 m/s over the entire pressure range.

Velocities traveling perpendicular to bedding increase more, and have more hysteresis, than those traveling parallel to bedding. $P_0^{o}$ increases from 0 to 50 MPa by 282 m/s and $P_{90}^{o}$ increases only by 144 m/s. This could suggest that porosity in the sample is aligned horizontally.

Figure 6 shows the five elastic constants estimated by using the measured velocities. Hysteresis is observed in these too as a consequence of hysteresis in the velocities. Figure 7 shows the anisotropic parameters as function of confining pressure. As microcracks and other porosity closes $\varepsilon$ and $\delta$ tend to stabilize with increasing pressure. If the main cause of anisotropy was preferred alignment of microcracks both $\varepsilon$ and $\delta$ would tend towards zero as pressure increase. Therefore, the latter indicate that the anisotropy in the sample mainly due to layering.

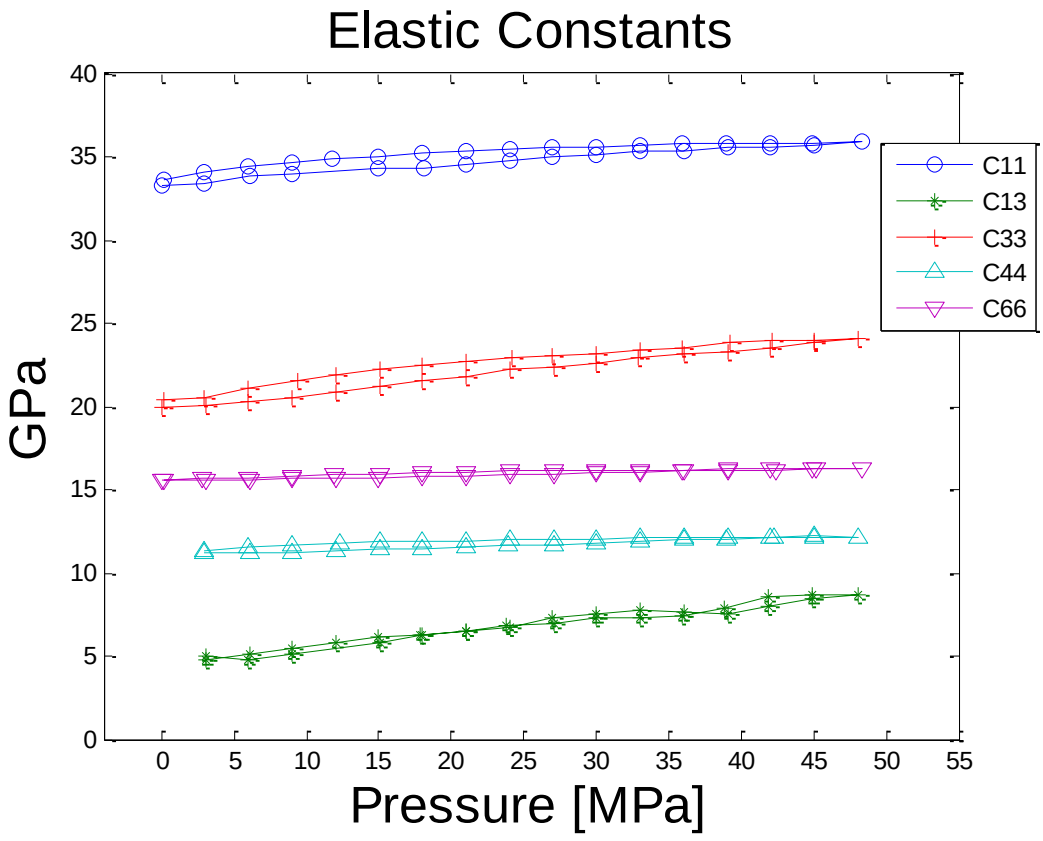


Figure 6. Estimated elastic constants from measured velocities.

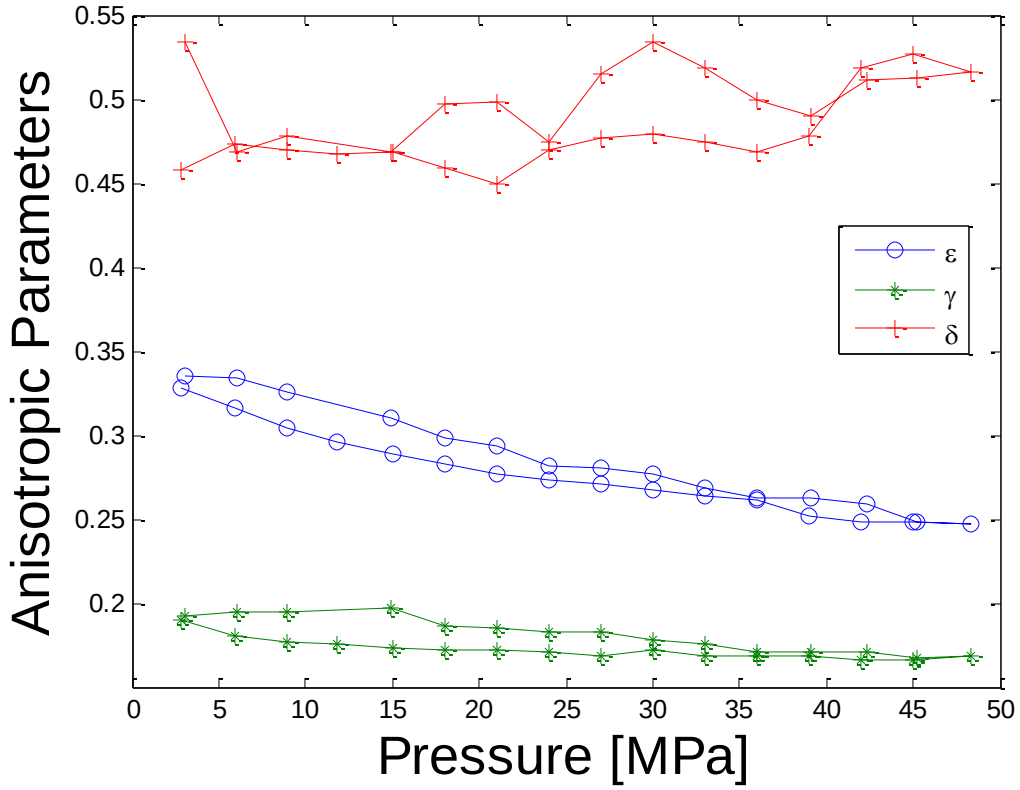


Figure 7. Anisotropic parameters.

## Conclusions

Results show that sample analyzed is anisotropic with vertical axis of symmetry. Analysis of velocities shows a dependence of travel times with confining pressure for both P- and S-waves. Pressurization and depressurization of samples show that microcracks and pores open and close at different rates for the same pressure (hysteresis). Microcracks have a minor role as a source of anisotropy, being anisotropy an intrinsic property of the sample due likely to layering.

Ultrasonic pulse transmission method along with multi-faced cube method is an elegant way to investigate elastic anisotropy in geological materials since it allows to simultaneously measure P- and S-waveforms in different directions from a single sample since it overcomes heterogeneities issues that can be present when using multi-core method.

Multifaced cube method can be a useful tool to investigate elastic anisotropy in shales (known as being strongly anisotropic) since these are present in most unconventional reservoirs where obtaining travel times in the direction parallel to bedding can be challenging from surface.

## Acknowledgements

The author thanks IMP (Instituto Mexicano del Petróleo) and the University of Alberta for supporting this research and to NSERC and the Canada Research Chairs program for financial assistance. Also thanks to Lucas Duerksen for his help in the Rock Physics Laboratory of the Experimental Geophysics Group (EGG) at the University of Alberta.

**References**


Cholach, P. Y., and Schmitt, D. R., 2006, Intrinsic elasticity of a textured transversely isotropic muscovite aggregate:Comparisons to the seismic anisotropy of schists and shales: J. Geophys. Res., **111**, 410-427.

Dey-Barsukov, S., Dürrast, H., Rabbel, W., Seigesmund, S., and Wende, S., 2000, Aligned fractures in carbonate rocks: laboratory and in situ measurements of seismic anisotropy: International Journal of Earth Sciences, **88**, 829-839.

Gardner, G. H. F., Wyllie, M. R. J., and Droschak, D. M., 1965, Hysteresis in the velocity-pressure characteristics of rocks: Geophysics, **30**, 111-116.

He, T., 2006, P- and S-wave velocity measurement and pressure sensitivity analysis of AVA response: M.Sc. thesis, University of Alberta.

Kebaili, A., and Schmitt, D. R., 1997, Ultrasonic anisotropic phase velocity determination with the Radon transform: The Journal of the Acoustical Society of America, **101- 6**, 3278–3286.

Kuster, G. T., and Toksöz, M. N., 1974, Velocity and attenuation seismic waves in twophase media: Part 1. Theoretical formulations: Geophysics, **39**, 587-606.

Mah, M., and Schmitt, D. R., 2001a, Experimental determination of the elastic coefficients of an orthorhombic material: Geophysics, **66,** 1217-1225.

Mah, M., and Schmitt, D. R., 2001b, Near point-source longitudinal and transverse mode ultrasonic arrays for material characterization: IEEE Transactions on Ultrasonics, Ferroelectrics, and Frequency Control, **48**, 691-698.

Meléndez, J. M., and Schmitt, D. R., 2011, Investigating anisotropy in rocks by using pulse transmission method, CSEG Recorder, **36-7**, 34-38.

Reinicke, A., Erik Rybacki, Stanchits, S., Huenges, E., and Dresen, G., 2010, Hydraulic fracturing stimulation techniques and formation damage mechanisms—Implications from laboratory testing of tight sandstone–proppant systems: Chemie der Erde **70 S3**, 107–117.

Thomsen, L., 1986, Weak elastic anisotropy: Geophysics, **51**, 1954-1966.

Vernik, L., and Liu, X., 1997, Velocity anisotropy in shales: A petrophysical study: Geophysics, **62**, 521-532.

Wang, Z., 2002b, Seismic anisotropy in sedimentary rocks, part 2: Laboratory data: Geophysics, **67**, 1423-1440

Zimmermann, G., and Reinicke, A., 2010, Hydraulic stimulation of a deep sandstone reservoir to develop an enhanced geothermal system: laboratory and field experiments: Geothermics, **39**, 70–77.